Journal of Power Sources 217 (2012) 345–350

Contents lists available at SciVerse ScienceDirect

Journal of Power Sources

journal homepage: www.elsevier.com/locate/jpowsour

On-board hydrogen production by hydrolysis from designed Al–Cu alloys and the application of this technology to polymer electrolyte membrane fuel cells

MinJoong Kim [a,b], KwangSup Eom [b], JaeYoung Kwon [c], EunAe Cho [b], HyukSang Kwon [a,*]

[a] Dept. of Materials Science and Engineering, Korea Advanced Institute of Science and Technology (KAIST), Daejeon 305-701, Republic of Korea
[b] Fuel Cell Center, Korea Institute of Science and Technology (KIST), Seoul 136-791, Republic of Korea
[c] Dept. of Materials Science and Engineering, University of Michigan, Ann Arbor, MI 48109, USA

HIGHLIGHTS

- Al–Cu (2–5 wt.%) alloys are designed for fast H_2 generation from hydrolysis.
- Designed Al–Cu alloys have noble Al_2Cu phase along the grain boundary.
- Al-5 wt.% Cu alloy exhibits about 5 times greater H_2 production rate than pure Al.
- It is due to the combined action of galvanic corrosion and intergranular corrosion.
- When supplying H_2 produced from this system to PEMFC, it is operated stably.

ARTICLE INFO

Article history:
Received 5 April 2012
Received in revised form
31 May 2012
Accepted 2 June 2012
Available online 12 June 2012

Keywords:
Aluminum copper alloy
Hydrolysis
On-board hydrogen production
Galvanic corrosion
Intergranular corrosion
Polymer electrolyte membrane fuel cells

ABSTRACT

Al–Cu alloys containing various amounts of Cu (2–5 wt.%) are designed to increase the hydrogen production rate in an alkaline solution by precipitating the electrochemically noble Al_2Cu phase along the grain boundary. All of the Al–Cu alloys exhibit a microstructure with Al_2Cu precipitates, which is electrochemically noble to Al in an alkaline solution, along the grain boundary. The hydrogen generation rate of Al–Cu alloys increases as the amount of Cu increases, and the Al- 5 wt.% Cu alloy exhibits a 4.7 times greater hydrogen generation rate than that of pure Al. This significant increase in hydrogen generation is affected by the combined action of galvanic corrosion and intergranular corrosion. When hydrogen produced by the hydrolysis of Al–Cu alloys is directly fed to a polymer electrolyte membrane fuel cell (PEMFC) anode, the cell voltage exhibits a stable value of approximately 0.73 V without a humidifier.

1. Introduction

An on-board hydrogen production system has many advantages in terms of supplying hydrogen because it eliminates the need for hydrogen storage. In the last ten years, chemical hydrides such as $NaBH_4$ [1–4], $LiBH_4$, $NaAlH_4$, and NH_3BH_3 [5–8] have received much attention as on-board hydrogen production materials due to their high hydrogen production density. However, their high cost has been a limiting factor for commercial applications. Recently, the on-board hydrogen production method involving the hydrolysis of electrochemically active metals, such as aluminum (Al [9–23], Na [24], Mg [25], Zn [26], etc.), have been studied by many researchers because they are more economical compared with chemical hydrides. Among the active metals, aluminum has a higher hydrogen production density (3.7 wt.% H_2) from hydrolysis than other active metals (Mg: 3.3 wt.% H_2, Na: 2.4 wt% H_2, Zn: 2.0 wt.% H_2) because it is light and has high oxidation states of +3. The reaction of Al hydrolysis in an alkaline solution can be expressed by Eq. (1) [9]:

$$Al + 3H_2O \rightarrow Al(OH)_3 + 3/2H_2 \quad (1)$$

In previous reports [9–23], most researchers have used Al or Al alloys in powder form for hydrolysis in alkaline and neutral solution, which yielded very high hydrolysis rates due to the large surface area of Al powders. However, it is very difficult to store the

* Corresponding author. Tel.: +82 42 350 3326; fax: +82 42 350 3310.
E-mail address: hskwon@kaist.ac.kr (H. Kwon).

0378-7753/$ – see front matter © 2012 Elsevier B.V. All rights reserved.
http://dx.doi.org/10.1016/j.jpowsour.2012.06.008

Al and Al alloy powders safely because they are explosive when in contact with moisture or a small amount of heat. In addition, they are quite expensive due to the complex manufacturing process required to produce them. Accordingly, the development of safe Al and Al alloys in bulk form with a high hydrogen generation rate has proven to be a challenge.

It is notable from Eq. (1) that the hydrogen generation rate is equivalent to the dissolution rate or corrosion rate of Al metal to Al ion (Al^{3+}). Accordingly, the corrosion rate of Al should be increased to increase the hydrogen generation rate from the hydrolysis reaction. Eom et. al. [27,28] have reported that fast hydrogen generation from the hydrolysis of Al in an alkaline solution was achieved by precipitating an electrochemically noble phase (Al_3Fe) along the grain boundaries in bulk Al–Fe alloy, thereby causing the combined action of galvanic corrosion and intergranular corrosion. Despite the fact that a small amount of Fe (1 wt.%) was alloyed with Al, the hydrogen generation rate was significantly increased 3.7 times than that of pure Al [27]. Furthermore, the on-board hydrogen production system using hydrolysis by bulk (sheet) Al–Fe alloy could be used to operate PEMFC stably, because it had enough hydrogen production kinetics despite the Al alloy was in bulk form (sheet) [29].

On the other hand, it is known that the Al_2Cu, Al_3Ni, Al_6Mn, or Al_8Mg_5 phases are also electrochemically noble intermetallic compounds of Al alloys [30]. Hence, the aforementioned alloys may also exhibit faster hydrogen production than pure Al via the above-mentioned strategy. In this work, Cu was used as the alloying element for Al for economic reasons. Cu is cheaper than different Al alloying elements such as Ni, Mn, and Mg. Moreover, the Al–Cu alloys is the best Al alloys to use practically because it is easy to obtain waste Al alloy scraps containing Cu with very low price from the fact that Cu is a major alloying element for most of the Al alloys. In addition, based on the phase diagram, the Al_2Cu phase can be easily precipitated along the grain boundary of the Al–Cu alloy [31]. In this present work, the effects of the amount of Cu in Al–Cu alloys on the microstructures and their hydrogen generation kinetics in an alkaline solution were examined to design Al–Cu alloys with a high hydrolysis rate from the combined action of galvanic corrosion and intergranular corrosion. The feasibility of the on-board production of hydrogen from the hydrolysis of Al–Cu alloys for PEMFCs was also investigated.

2. Experimental

2.1. Preparation of materials

Al–Cu alloys containing various amounts of Cu (0–5 wt.% Cu) were prepared from commercial pure Al (99.9%) and Al–Cu master alloy (Al_2Cu). To fabricate casting Al-xCu alloys ($x = 2$–5 wt.%), pure Al and the Al–Cu master alloy were melted at 800 °C. Afterward, the fused alloys were poured into a stainless steel mold and air cooled to 20 °C in the mold. The specimens for the hydrogen generation test were prepared by cutting the bulk form into $2 \times 2 \times 1$ cm^3 samples. The exposed surface area of all of the specimens was kept constant at 16 cm^2.

2.2. Measurement of the hydrogen generation rate

The hydrogen generation test was performed in 50 ml of 10 wt.% NaOH solution at 30 °C. The volume of hydrogen gas generated from the hydrolysis of the Al–Cu alloys was measured by a mass flow meter (MFM). The reactor was immersed in a water bath to keep the solution temperature constant, and no stirring was performed in the reactor.

2.3. Physical and electrochemical analysis

The surface morphologies, chemical compositions, and phase structures of the Al–Cu alloys were analyzed using scanning electron microscopy (SEM), energy dispersive spectroscopy (EDS), and X-ray diffraction (XRD). The electrochemical properties, such as the polarization behavior and the galvanic corrosion of the Al–Cu alloys, were analyzed by a potentiodynamic (PD) test and a zero resistance ammeter (ZRA) test using a potentiostat (EG &G 273).

2.4. PEMFC single-cell preparation and operation

The feasibility of on-board hydrogen production from the hydrolysis of Al–Cu alloys in a PEMFC was investigated by a single-cell test. A single cell was assembled with a commercial membrane electrode assembly (MEA, GORE™), gas diffusion layers (GDL, SGL 10 BC), graphite bipolar plates with serpentine flow fields, and aluminum end plates. The geometric active area of the MEA was 5×5 cm^2, and the Pt loading in the catalyst layer was 0.4 mg cm^{-2}. To activate the MEA, the assembled single cell was operated at 0.4 V for 24 h using hydrogen and air with an RH of 100%. After the activation process, the anode inlet of the single cell was connected directly with the hydrogen generation reactor, and then hydrogen gas generated from the hydrolysis of Al–Cu alloys was fed to the anode.

3. Results and discussion

3.1. Microstructures of Al–Cu alloys

Fig. 1 shows the surface morphologies of the Al-x wt.% Cu alloys ($x = 2, 3, 5$) after chemical etching for 30 s in Kroll's reagent (92 ml D.I. water + 6 ml HNO_3 + 2 ml HF). All of the Al–Cu alloys have some precipitates formed along the grain boundary, but there are some morphology changes as the amount of Cu increases. As the amount of Cu in the Al–Cu alloy increases, the amount of precipitates increases, and the average grain size becomes smaller from about 100 to 50, 30 μm. As shown in Fig. 1(d), the gray grain region was composed of only 100 at.% Al, and the white precipitates along the grain boundary were composed of 81.2 at.% Al and 18.8 at.% Cu, based on the EDS results. The white precipitate is predicted to be the eutectic that forms in between the dendrites as fine lamellae of Al and Al_2Cu because Al_2Cu is the only intermetallic compound in the Al and Cu binary alloy system, based on the phase diagram. The phase structure of the precipitate was confirmed by XRD analysis. Fig. 2 shows the XRD pattern of the Al-5 wt.% Cu alloy at $2\theta = 20$–70°. Except for peaks corresponding to Al, some peaks corresponding to Al_2Cu phase were detected at $2\theta = 20$–50°, as expected.

3.2. Electrochemical analysis of the Al–Cu alloys

Galvanic corrosion [32] occurs when two dissimilar metals with different corrosion potentials (E_{corr}) are connected electrically in a solution. Then, the electrochemically active metal or the metal with a lower corrosion potential is corroded preferentially, while the electrochemically noble metal is protected from corrosion. Furthermore, as the difference in the corrosion potential between two dissimilar metals increases, the corrosion rate of the more active metal increases. Fig. 3(a) shows potentiodynamic polarization curves of the Al and Al_2Cu phases measured in 0.1 M NaOH solution at 30 °C. As shown in Fig. 3(a), the corrosion potential (E_{corr}) of the Al_2Cu phase is −1.3 $V_{SCE,}$ which is 0.49 V more noble than the E_{corr} of Al (−1.79 V_{SCE}). Therefore, the Al phase acts as an anode site, and the Al_2Cu phase acts as a cathode site to generate hydrogen gas in the Al–Cu alloys, which may accelerate the corrosion rate of Al. The measured corrosion current densities of

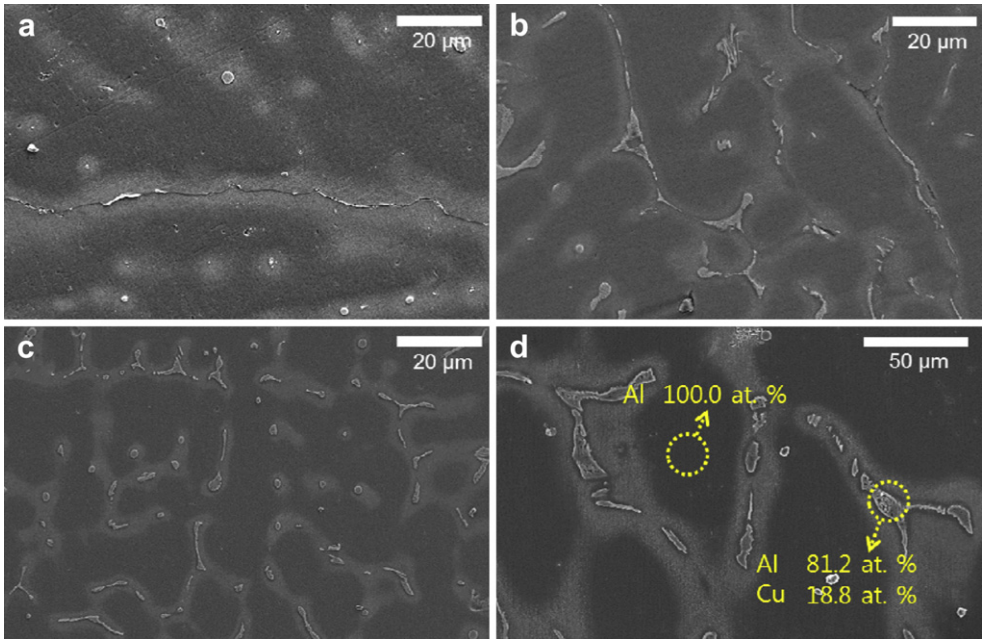

Fig. 1. SEM images of Al-x wt.% Cu (x = (a) 2 wt.%, (b) 3 wt.%, (c)–(d) 5 wt.%) after chemical etching for 30 s in Kroll's reagent.

the Al and Al_2Cu phases are i_{corr} (Al) = 1.98 mA cm^{-2} and i_{corr} (Al_2Cu) = 1.24 mA cm^{-2}. The Al_2Cu phase is more stable in an alkaline solution than the Al phase. To confirm the effects of galvanic corrosion between Al and Al_2Cu precipitates in the Al–Cu alloy, a ZRA test was conducted in a 0.1 M NaOH solution at 30 °C. As shown in Fig. 3(b), the current density due to hydrogen generation on the cathodic site was increased from 1.98 (i_{corr} (Al)) to 3.80 mA cm^{-2} (i_{couple} (Al–Al_2Cu)) by galvanic coupling of the Al phase to the Al_2Cu phase. The current density is 1.9 times greater than that of pure Al without galvanic coupling of the Al and Al_2Cu phases. Therefore, it is expected that the hydrogen generation rate from hydrolysis would be increased approximately 1.9 times by the effects of galvanic corrosion between Al and Al_2Cu precipitates in the Al–Cu alloys.

3.3. Hydrogen generation kinetics of Al–Cu alloys

Fig. 4 shows the effects of the amount of Cu in Al–Cu alloys on the hydrogen generation kinetics of the hydrolysis reaction in

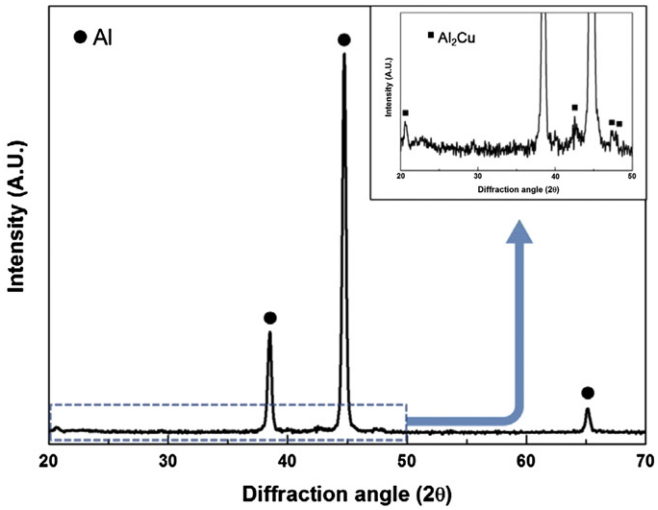

Fig. 2. XRD patterns of the Al-5 wt.% Cu alloy.

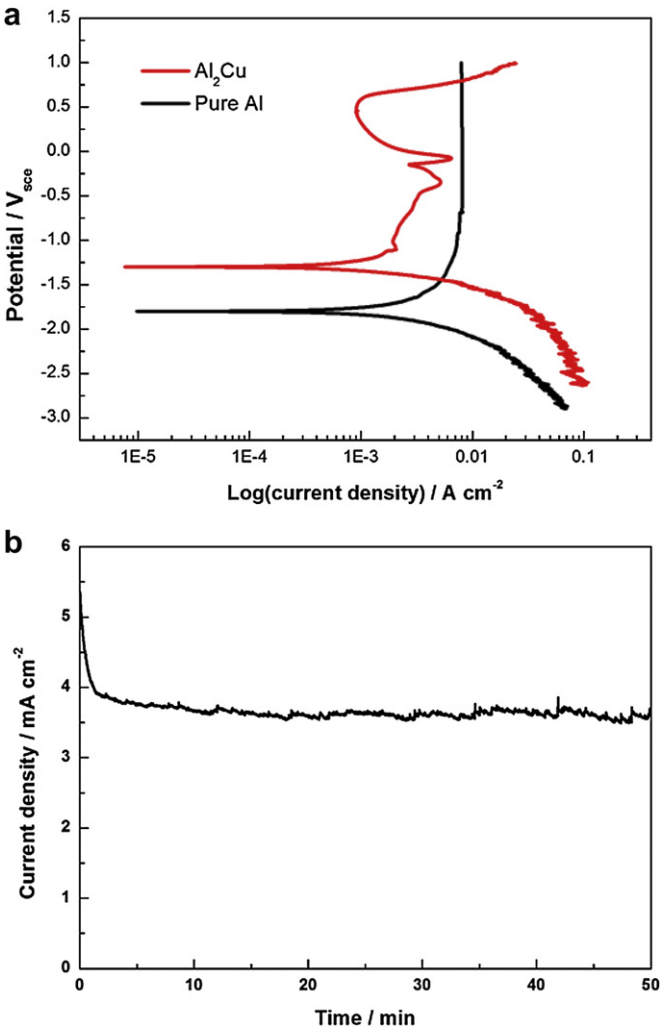

Fig. 3. (a) The potentiodynamic polarization curve of pure Al (99.9%) and Al_2Cu at 30 °C in a 0.1 M NaOH solution. (b) The zero resistance ammeter (ZRA) curve for pure Al (99.9%) and Al_2Cu at 30 °C in a 0.1 M NaOH solution for the galvanic corrosion test.

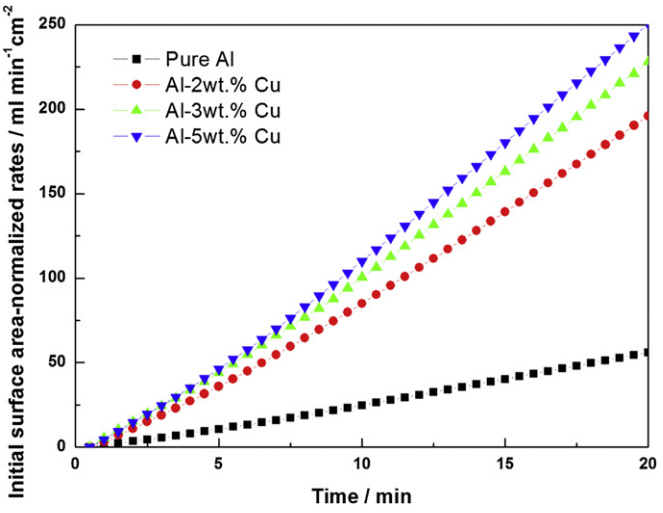

Fig. 4. Effects of the amount of Cu on the hydrogen generation kinetics for the hydrolysis of Al-x wt.% (x = 0, 2, 3, and 5) Cu alloys in a 10 wt.% NaOH solution at 30 °C.

Table 1
The average hydrogen generation rates over 20 min as a function of the initial surface area of the Al–Cu alloys containing various amounts of Cu (0–5 wt.%) from the hydrolysis reaction in a 10 wt.% NaOH solution at 30 °C.

Samples	Average hydrogen generation rate/ml min^{-1} cm^{-2}
Al	2.8
Al-2 wt.% Cu	9.8
Al-3 wt.% Cu	11.4
Al-5 wt.% Cu	12.5

a 10 wt.% NaOH solution at 30 °C. The average hydrogen generation rates over 20 min as a function of the initial surface area of the Al–Cu alloys containing various amounts of Cu (0–5 wt.%) are reported in Table 1. As shown in Fig. 4, as the amount of Cu in the Al–Cu alloys was increased from 0 to 2, 3, and 5 wt.%, the average hydrogen generation rate from Al hydrolysis significantly increased from 2.80 to 9.80, 11.41, and 12.53 ml min^{-1} cm^{-2}. The hydrogen generation rate of Al-5 wt.% Cu alloy is 4.7 times higher than that of pure Al, and it is much greater than the increase in the ratio of the cathodic current density corresponding to the generation of hydrogen caused by the galvanic coupling of the Al and Al_2Cu phases (1.9 times). The rate is also greater than previous results using an Al–Fe alloy (3.7 times) [27]. The Al-2 and 3 wt.% Cu alloys also exhibited a greater increase in the hydrogen generation rate than the galvanic corrosion test results: 3.7 and 4.3 times, respectively. Accordingly, it is assumed that the hydrolysis of Al–Cu alloys would be affected by not only galvanic corrosion between Al and Al_2Cu precipitates within the Al–Cu alloys but also by increases in the reaction area due to intergranular corrosion along grain boundaries. The corrosion behavior of the Al–Cu alloys in the alkaline solution will be discussed in detail.

3.4. Corrosion behavior of Al–Cu alloys during hydrolysis

Fig. 5 shows SEM images of Al and Al–Cu alloys after hydrolysis for 10 min in a 10 wt.% NaOH solution at 30 °C. As shown in Fig. 5(a), the Al shows a smoothly dissolved surface with randomly distributed shallow holes. In contrast, the Al–Cu alloys (Fig. 5(b)–(d)) show cracked structures along the grain boundary due to intergranular corrosion during the hydrolysis reaction. The reason why intergranular corrosion occurs in the Al–Cu alloys is that the Al phase near the Al_2Cu phase that precipitated along the grain boundaries was preferentially dissolved during the hydrolysis reaction due to galvanic coupling of Al (anode) and the noble precipitate (cathode). The cracks that formed along the grain boundaries via intergranular corrosion propagated into the Al–Cu alloys as the hydrolysis time increased, as shown in Fig. 6(a). As the hydrolysis time increased further, wide and deep cracks approximately 200 μm wide were formed with a large exposure area, as shown in Fig. 6(b). It is assumed that the production and propagation of cracks due to intergranular corrosion could induce an increase in the hydrolysis rate by increasing the exposed reaction

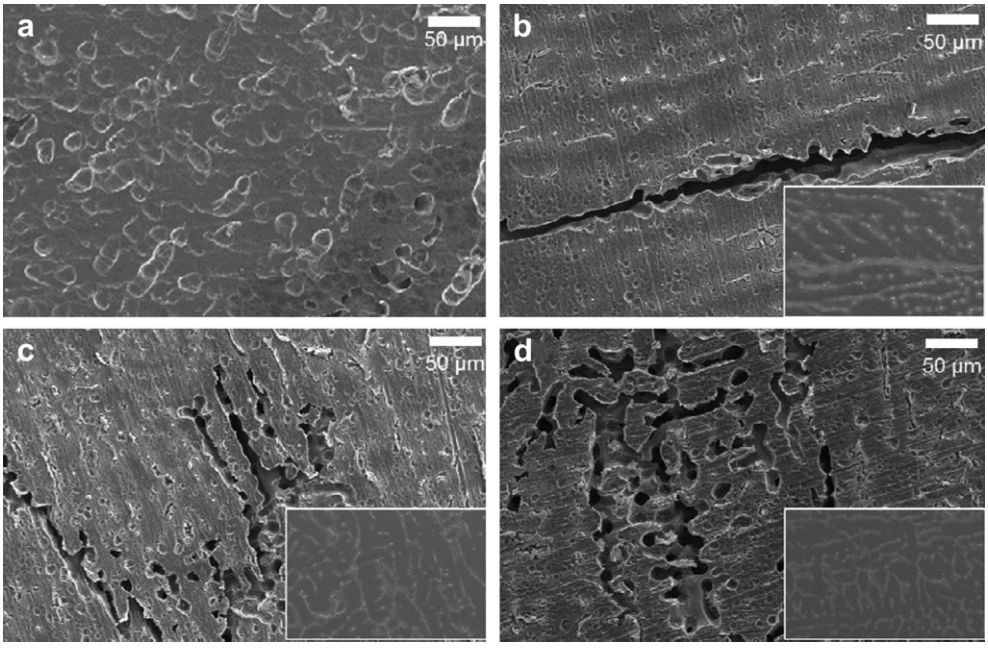

Fig. 5. SEM images of Al-x wt.% Cu (x = (a) 0 wt.%, (b) 2 wt.%, (c) 3 wt.%, and (d) 5 wt.%) after hydrolysis for 10 min in a 10 wt.% NaOH solution at 30 °C.

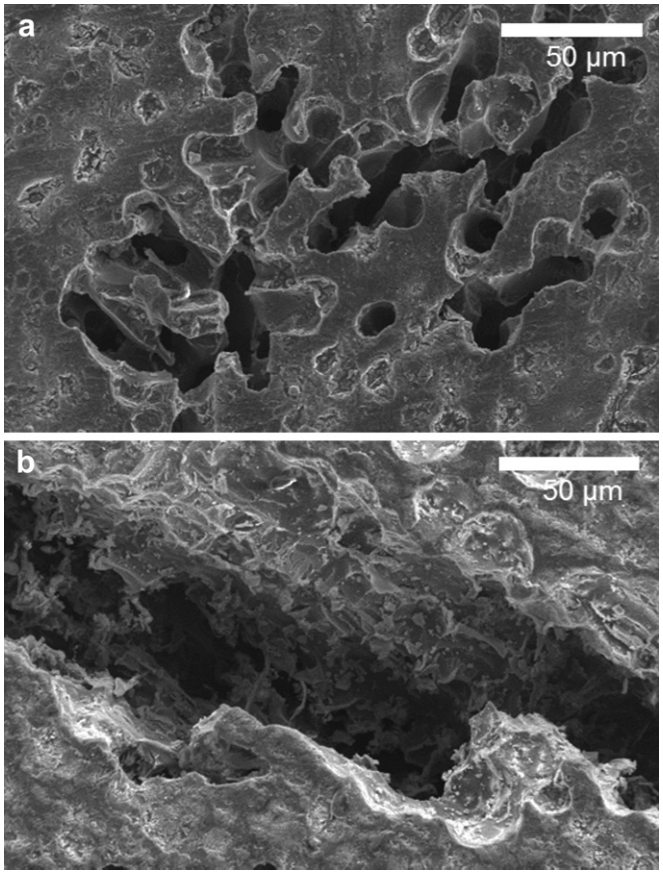

Fig. 6. SEM images of Al-5 wt.% Cu after hydrolysis for (a) 15 min and (b) 30 min in a 10 wt.% NaOH solution at 30 °C.

area. As discussed in Section 3.1, the amount of precipitates along the grain boundary increased as the amount of Cu increased, which led to an increase in the contact area between the Al and Al_2Cu precipitates in the Al–Cu alloys. Therefore, the significant increase in the hydrogen generation rate of Al-5 wt.% Cu alloy is due to the combined action of galvanic corrosion and increased intergranular corrosion due to the large contact area between Al and Al_2Cu precipitates. The effects of galvanic corrosion on the hydrogen generation rate would be equal for all of the Al–Cu alloys, but the effects of intergranular corrosion could vary as a function of the microstructure changes caused by the changes in the amount of Cu.

3.5. PEMFC operation

Fig. 7(a) shows the current–voltage (I–V) curve of a single PEM cell operated from supplying the hydrogen generated from the hydrolysis of a 14-g sheet of Al–Cu alloy in a 10 wt.% NaOH solution at 40 °C. The cell voltage is 0.74 V at 10 A without humidification. Fig. 7(b) shows the cell voltage curves at a constant load of 10 A for the single cell at the same hydrogen supply conditions. The cell voltage exhibited a stable value of approximately 0.73 V for 32 min. After that, the cell voltage decreased slightly from 0.73 to 0. 67 V for about 5 min and then decreased drastically to 0 V for a few min. This might decrease the hydrogen generation rate to below SR 1.0 (116 ml min^{-1}) after approximately 35 min [29]. However, the designed Al–Cu alloys in this study have high enough hydrogen production rates to operate a PEMFC successfully without a humidifier. The utilization ratio of the Al–Cu alloys to the quantity of electricity was calculated to about 16.1%.

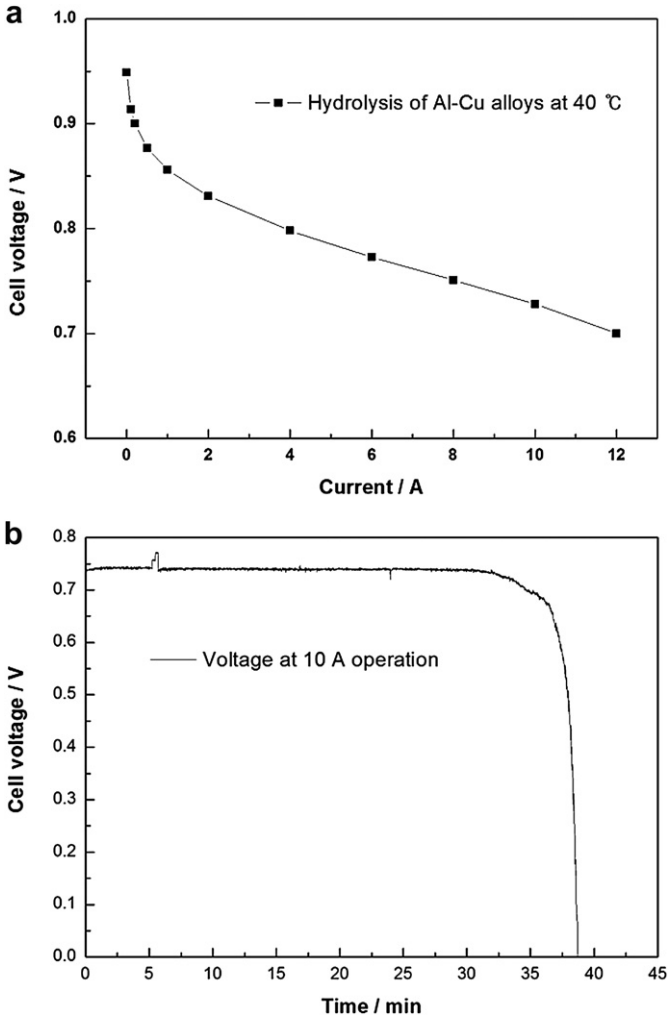

Fig. 7. (a) The I–V curve and (b) the cell voltage profile measured at a constant current load (10 A) for a PEMFC single cell when hydrogen generated by the hydrolysis of Al–Cu alloys is directly fed to the PEMFC anode.

4. Conclusions

Al–Cu alloys containing various amounts of Cu were designed to achieve a fast hydrogen generation rate in an alkaline solution by precipitating the electrochemically noble Al_2Cu phase along the grain boundary. The amount of Al_2Cu precipitates increased and the grain size became smaller as the amount of Cu increased. The Al_2Cu phase is nobler than Al in the alkaline solution. The corrosion potentials (E_{corr}) of the Al_2Cu and Al phases are −1.3 V_{SCE} and −1.79 V_{SCE}, respectively, in a 0.1 M NaOH solution at 30 °C. The cathodic current density corresponding to the generation of hydrogen was increased 1.9 times higher than the pure Al by galvanic coupling of the Al and Al_2Cu phases. The Al-5 wt.% Cu alloy exhibited a 4.7 times higher hydrogen generation rate than that of pure Al in a 10 wt.% NaOH solution at 30 °C. This excellent hydrogen generation rate of the Al–Cu alloys results from the combined effects of galvanic corrosion and increased intergranular corrosion due to the large contact area between the Al and Al_2Cu precipitates. The contribution of galvanic corrosion is equal in all of the Al–Cu alloys, but the magnitude of the intergranular corrosion varied with the microstructure changes that were caused by changes in the amount of Cu. When the hydrogen generated by the hydrolysis of Al–Cu alloys is directly fed to a PEMFC anode, the cell voltage exhibited

a stable value of approximately 0.74 V without a humidifier. Therefore, an on-board hydrogen production method using the hydrolysis of the Al alloys described in this study could be designed for successful PEMFC operation.

Acknowledgments

This work was financially supported for the Korea Institute of Energy Technology Evaluation and Planning (KETEP) funded by the Ministry of Knowledge Economy.

References

[1] H.I. Schlesinger, H.C. Brown, A.E. Finholt, J.R. Gilbreath, H.R. Hoekstra, E.K. Hyde, J. Am. Chem. Soc. 75 (1953) 215–219.
[2] S.C. Amendola, S.L. Sharp-Goldman, M.S. Janjua, N.C. Spencer, M.T. Kelly, P.J. Petillo, M. Binder, Int J. Hydrogen Energy 25 (2000) 969–975.
[3] Y. Kojima, K.-i. Suzuki, K. Fukumoto, M. Sasaki, T. Yamamoto, Y. Kawai, H. Hayashi, Int. J. Hydrogen Energy 27 (2002) 1029–1034.
[4] K. Eom, H. Kwon, Int. J. Hydrogen Energy 35 (2010) 5220–5226.
[5] M. Chandra, Q. Xu, J. Power Sources 156 (2006) 190–194.
[6] M.C. Denney, V. Pons, T.J. Hebden, D.M. Heinekey, K.I. Goldberg, J. Am. Chem. Soc. 128 (2006) 12048–12049.
[7] C.F. Yao, L. Zhuang, Y.L. Cao, X.P. Ai, H.X. Yang, Int. J. Hydrogen Energy 33 (2008) 2462–2467.
[8] K. Eom, K. Cho, H. Kwon, Int. J. Hydrogen Energy 35 (2010) 181–186.
[9] D. Belitskus, J. Electrochem. Soc. (1970). Other Information: See PB–230845, Medium: X.
[10] H. Hu, M. Qiao, Y. Pei, K. Fan, H. Li, B. Zong, X. Zhang, Appl. Catalysis A: General 252 (2003) 173–183.
[11] T. Hiraki, M. Takeuchi, M. Hisa, T. Akiyama, Mater. Trans. 46 (2005) 1052–1057.
[12] M.-Q. Fan, F. Xu, L.-X. Sun, Int. J. Hydrogen Energy 32 (2007) 2809–2815.
[13] A. Kundu, J.H. Jang, J.H. Gil, C.R. Jung, H.R. Lee, S.H. Kim, B. Ku, Y.S. Oh, J. Power Sources 170 (2007) 67–78.
[14] S.S. Martínez, L. Albañil Sánchez, A.A. Álvarez Gallegos, P.J. Sebastian, Int. J. Hydrogen Energy 32 (2007) 3159–3162.
[15] L. Soler, J. Macanas, M. Munoz, J. Casado, J. Power Sources 169 (2007) 144–149.
[16] L. Soler, J. Macanás, M. Muñoz, J. Casado, Int. J. Hydrogen Energy 32 (2007) 4702–4710.
[17] C.R. Jung, A. Kundu, B. Ku, J.H. Gil, H.R. Lee, J.H. Jang, J. Power Sources 175 (2008) 490–494.
[18] E.-D. Wang, P.-F. Shi, C.-Y. Du, X.-R. Wang, J. Power Sources 181 (2008) 144–148.
[19] L. Soler, A.M. Candela, J. Macanás, M. Muñoz, J. Casado, J. Power Sources 192 (2009) 21–26.
[20] H.Z. Wang, D.Y.C. Leung, M.K.H. Leung, M. Ni, Renewable Sustainable Energy Rev. 13 (2009) 845–853.
[21] W. Wang, D.M. Chen, K. Yang, Int. J. Hydrogen Energy 35 (2010) 12011–12019.
[22] J.T. Ziebarth, J.M. Woodall, R.A. Kramer, G. Choi, Int. J. Hydrogen Energy 36 (2011) 5271–5279.
[23] S. Liu, M.-q. Fan, C. Wang, Y.-x. Huang, D. Chen, L.-q. Bai, K.-y. Shu, Int. J. Hydrogen Energy 37 (2012) 1014–1020.
[24] F. Herzog, D. Glaubitz, Int. J. Hydrogen Energy 15 (1990) 13–19.
[25] M.H. Grosjean, M. Zidoune, L. Roué, J.Y. Huot, Int. J. Hydrogen Energy 31 (2006) 109–119.
[26] K. Wegner, H.C. Ly, R.J. Weiss, S.E. Pratsinis, A. Steinfeld, Int. J. Hydrogen Energy 31 (2006) 55–61.
[27] K.S. Eom, J.Y. Kwon, M.J. Kim, H.S. Kwon, J. Mater. Chem. 21 (2011) 13047–13051.
[28] K. Eom, M. Kim, S. Oh, E. Cho, H. Kwon, Int. J. Hydrogen Energy 36 (2011) 11825–11831.
[29] K. Eom, E. Cho, H. Kwon, Int. J. Hydrogen Energy 36 (2011) 12338–12342.
[30] ASTM (G62), Annual Book of ASTM Standards, ASTM International, USA, 1998.
[31] H. Okamoto, Phase Digrams for Binary Alloys, ASM International, USA, 2000, p. 31.
[32] D.A. Jones, Principles and Prevention of Corrosion, Prentice Hall, USA, 1996, p. 168.